HHS Public Access

Author manuscript

Radiology. Author manuscript; available in PMC 2017 January 10.

Published in final edited form as:

Radiology. 2017 January ; 282(1): 194–201. doi:10.1148/radiol.2016152387.

In Vivo ^{19}F MR Imaging Cell Tracking of Inflammatory Macrophages and Site-specific Development of Colitis-associated Dysplasia

Soo Hyun Shin, MS[1], **Deepak K. Kadayakkara, MD, PhD**, and **Jeff W. M. Bulte, PhD**

Cellular Imaging Section and Vascular Biology Program, Institute for Cell Engineering (S.H.S., D.K.K., J.W.M.B.), Russell H. Morgan Department of Radiology and Radiological Science, Division of MR Research (S.H.S., D.K.K., J.W.M.B.), Department of Oncology (D.K.K., J.W.M.B.), Department of Biomedical Engineering (S.H.S., J.W.M.B.), and Department of Chemical & Biomolecular Engineering (J.W.M.B.), The Johns Hopkins University School of Medicine, 217 Traylor Bldg, 720 Rutland Ave, Baltimore, MD 21205

Abstract

Purpose—To investigate whether the magnitude of in vivo fluorine 19 (^{19}F) magnetic resonance (MR) imaging signal is associated with subsequent development of colitis-associated dysplasia after in situ fluorination of inflammatory macrophages in a mouse model of inflammatory bowel disease (IBD).

Materials and Methods—Experiments were approved by the institutional animal care and use committee. Mice in the experimental group (n = 10) were administered azoxymethane and dextran sulfate sodium to induce colitis-associated dysplasia. Five mice were in the noninduced control group. Animals were injected with a commercially available perfluorocarbon and were examined in vivo with an 11.7-T MR imager for up to 110 days. Colons were then harvested followed by high-spatial-resolution ex vivo MR imaging. Multiple colon segments with or without ^{19}F signal were histologically graded and were correlated with ^{19}F signal intensity by using a Spearman correlation test. The signal intensity in mice with colitis-associated dysplasia was compared with that in control mice with a two-tailed Mann-Whitney U test.

Address correspondence to J.W.M. (jwmbulte@mri.jhu.edu).

[1]**Current address:** Molecular Imaging & Therapy Branch, Division of Convergence Technology, National Cancer Center, Goyang, Gyeonggi-do, Korea.

S.H.S. and D.K.K. contributed equally to this work.

Online supplemental material is available for this article.

Author contributions:

Guarantors of integrity of entire study, all authors; study concepts/study design or data acquisition or data analysis/interpretation, all authors; manuscript drafting or manuscript revision for important intellectual content, all authors; approval of final version of submitted manuscript, all authors; agrees to ensure any questions related to the work are appropriately resolved, all authors; literature research, all authors; experimental studies, all authors; statistical analysis, S.H.S., J.W.M.B.; and manuscript editing, all authors

Disclosures of Conflicts of Interest

S.H.S. disclosed no relevant relationships. **D.K.K.** disclosed no relevant relationships. **J.W.M.B.** Activities related to the present article: disclosed no relevant relationships. Activities not related to the present article: received a grant from Philips Healthcare. Other relationships: disclosed no relevant relationships.

Results—Patchy distributions of ^{19}F signal intensity in the colon wall were seen on in vivo and ex vivo images, representing chronic inflammation as shown by immunohistochemistry. Histologic scores of inflammation and site-specific development of colitis-associated dysplasia in the descending colon showed good correlation with normalized ^{19}F signal intensity ($r = 0.88$, $P = .033$ for the ascending colon; $r = 0.82$, $P = .006$ for the descending colon). A significantly ($P = .002$) higher normalized ^{19}F signal-to-noise ratio was found at sites that developed dysplasia (mean, 0.58 ± 0.09 [standard deviation]) as compared with sites that did not (mean, 0.17 ± 0.22).

Conclusion—^{19}F MR imaging cell tracking of macrophages can be used to assess local inflammation in a mouse model of IBD. The resulting local ^{19}F signal intensity, representing the magnitude of inflammation, has a positive correlation with the development of colitis-associated dysplasia.

The causal relationship between inflammation and cancer is well established (1). Epidemiologic studies in patients and in genetically modified mice have shown that chronic inflammation increases the risk of developing many types of cancer, including bladder, cervical, gastric, intestinal, and thyroid cancer (2,3). From a molecular perspective, transcription factors, such as nuclear factor κ-light-chain-enhancer of activated B cells (or NF-κB), signal transducer and activator of transcription 3 (or STAT3), and hypoxia-inducible factor 1-α (or HIF1α), in tumor cells recruit inflammatory cells, which then promote angiogenesis, tumor cell proliferation, survival, migration, and metastasis (3–5). It has been estimated that underlying inflammation is linked to 15%–20% of cancer mortality worldwide, and appropriate treatment with anti-inflammatory agents has been shown to decrease the incidence and mortality of several types of tumors (6,7).

Colitis-associated cancer is a subtype of colorectal cancer, with more than 1 million cases per year, that contributes substantially to overall cancer mortality (8). Colitis-associated cancer is a complication of inflammatory bowel disease (IBD), such as ulcerative colitis or Crohn disease, both of which are prevalent intestinal disorders in the United States (9,10). The chronic inflammation associated with IBD is characterized by infiltrating immune cells producing proinflammatory cytokines, which facilitate mutations in oncogenes and tumor suppressor genes, such as p53, adenomatous polyposis coli, and *KRAS* (11). Sustained inflammation accumulates these mutations in colonic epithelial cells, leading to the development of colitis-associated dysplasia, which is a precursor of colitis-associated cancer, through an inflammation-dysplasia-carcinoma sequence (12). Previously, Rutter et al (13) showed that the risk of colitis-associated cancer is directly correlated with duration of IBD and severity of inflammation. Hence, longitudinal monitoring of the location and severity of inflammation may enable earlier diagnosis and treatment of colitis-associated cancer.

Diagnosis of IBD is most commonly based on colonoscopy and mucosal biopsy findings, which are invasive methods that cause patient discomfort, damage colon tissue, and generate sampling errors. To overcome these limitations, noninvasive imaging techniques, such as computed tomography and magnetic resonance (MR) imaging, have been studied (14,15). These techniques are often referred to as *virtual colonography*. However, conventional hydrogen 1 (^{1}H) MR imaging of the bowel is not specific for inflammation but is based on three-dimensional anatomy and volumetry measurement of colon wall thickness (13).

MR imaging can be used to track inflammation by using superparamagnetic iron oxide nanoparticles that are taken up by macrophages (16,17). More recently, fluorine 19 (^{19}F) MR imaging with perfluorocarbon (PFC) emulsions similarly has been used as a noninvasive imaging method to depict inflammatory sites in a variety of organs and tissues (18–23). This method is based on in situ labeling of macrophages, which phagocytose the injected PFCs (24). PFCs are biologically inert inorganic molecules (25), and the absence of endogenous ^{19}F in biologic tissues ensures that the signals originating from labeled cells create so-called hot-spot images (26–29). As compared with hypointense superparamagnetic iron oxide–induced signal changes, these ^{19}F tracer-specific patches of signal are particularly well suited for imaging bowel inflammation, since bowel movements and the presence of air pockets that cause nonspecific signal hypointensities have precluded the use of superparamagnetic iron oxide for this application. Since macrophages are crucial mediators of chronic inflammation in patients with IBD (30,31), selective labeling of macrophages enables one to image inflammatory loci with high specificity (18). Furthermore, ^{19}F MR imaging can be used to quantify ex vivo–labeled cells (32). Hence, it may be used to score the local macrophage load and thus the severity of inflammation (33). Importantly, the method may be clinically applicable, as PFC-based ^{19}F MR imaging cell tracking studies have been performed in patients (34). After in situ fluorination of inflammatory macrophages in a mouse model of IBD, we investigated whether in vivo ^{19}F MR imaging signal intensity was associated with subsequent development of colitis-associated dysplasia.

Materials and Methods

Mouse Model of Colitis-associated Dysplasia

All experimental procedures involving animals were approved by our institutional animal care and use committee. Colitis-associated dysplasia was induced in mice, as previously described (35,36). Colitis-associated dysplasia developed over 7 weeks, after which time the animals were observed with MR imaging for 9 weeks (Fig E1 [online]). To this end, 10 8-week-old female A/J mice were purchased from Jackson Laboratory (Bar Harbor, Me) and were intraperitoneally injected with azoxymethane (10 mg per kilogram of body weight, Sigma, St Louis, Mo) at day 0. To ensure that tumors developed through IBD, dextran sulfate sodium (MP Biomedicals, Solon, Ohio) was used to induce chronic colon inflammation. Dextran sulfate sodium was dissolved in drinking water (2.5% weight per volume). Each dextran sulfate sodium cycle lasted 1 week and was repeated every 3 weeks until week 7. Usually, three to 10 macroscopic lesions develop in 80%–100% of the animals. Mice that did not receive azoxymethane and dextran sulfate sodium served as the control group ($n = 5$). Body weight was recorded every week until all experimental and control animals were sacrificed at day 110 after azoxymethane injection. Mice were fed a standard diet without supplements (global 18% extruded rodent diet [2018SX; Teklad, Indianapolis, Ind] containing no less than 18% crude protein, no less than 5% fat, and not more than 5% fiber).

In Vivo MR Imaging

Two days before beginning the MR imaging studies, 200 μL of PFC emulsion (Celsense, Pittsburgh, Pa) was injected intravenously via a tail vein with a 27-gauge needle. The concentration of PFC emulsion was 200 mg/mL, and the diameter of the emulsion ranged from 145 to 165 nm according to the manufacturer. For immunostaining, five animals were injected with a fluorescent version of the same emulsion (VS-1000H DM Red; Celsense) with the same experimental parameters.

Five mice were imaged every 15 days from day 50 to day 110 (Fig E1 [online]). The five remaining mice and mice in the control group were imaged two times until day 65. Imaging was performed by using an 11.7-T horizontal MR imager (BioSpec 117/16 USR; Bruker Biospin, Billerica, Mass) with a 20-mm surface coil tunable to both ^{1}H and ^{19}F frequencies. Mice were anesthetized with 1.5% isoflurane gas, and ^{1}H images were acquired by using a rapid acquisition with refocused echoes (RARE) sequence with the following parameters: repetition time msec/echo time msec, 1200/30; section thickness, 2 mm; matrix, 256 × 256; RARE factor, eight; field of view, 3.2 × 2.0 cm; and four signals acquired. ^{19}F images were acquired by using the RARE sequence and the following parameters: 1000/14; section thickness, 2 mm; matrix, 64 × 32; RARE factor, eight; field of view, 3.2 × 2.0 cm; and 64 sections acquired. ^{19}F images were expressed in pseudocolor scale and were coregistered to the corresponding ^{1}H images by using Paravision software (version 5.1; Bruker Biospin, Ettlingen, Germany). Each image was scaled for subjective optimal visualization and presentation.

Ex Vivo MR Imaging

After the last in vivo MR imaging time point, all mice were euthanized, and the colons were excised. Ex vivo MR imaging was performed to confirm the results from in vivo MR imaging with higher resolution to precisely colocalize the inflammatory sites and dysplastic lesions with ^{19}F signal intensity. Each colon was divided into two parts, the ascending colon and the descending colon, and a glass rod was inserted into the lumen of each colon segment to straighten the tissue. After fixation in 4% paraformaldehyde for 2 days, tissues were transferred to 10-mmol/L phosphate-buffered saline solution with a pH of 7.4 and were imaged with a 17.6-T vertical bore MR imager (Bruker Biospin) and a 25-mm volume coil tunable to either ^{1}H or ^{19}F. ^{1}H and ^{19}F images were again acquired by using the RARE sequence. The ^{1}H MR imaging parameters were as follows: 1000/10; section thickness, 1 mm; matrix, 256 × 256; RARE factor, eight; field of view for sagittal images, 2.6 × 1.3 cm; field of view for axial images, 1.3 × 1.3 cm; and four signals acquired. The ^{19}F MR imaging parameters were as follows: 1000/6: matrix, 64 × 32; RARE factor, 16; and 256 signals acquired. ^{19}F images were superimposed on the corresponding ^{1}H images.

^{19}F MR Signal Intensity Analysis

We used ParaVision 5.1 software (Bruker Biospin) to analyze ^{19}F MR signal intensity. Free-form polygonal regions of interest (ROIs) ranging from 3 to 10 mm were drawn by an investigator (S.H.S.) in a nonblinded fashion over every ^{19}F signal intensity patch in the ascending and descending colon, with two to four ROIs per mouse. Since excised colon segments were used, the ROIs could be easily drawn on both the ascending colon and the

descending colon. ROIs were not drawn for control mice since the ^{19}F signal intensity in the colon is absent for this group. The aforementioned software was used to measure mean signal intensity and the standard deviation of the background signal intensity to calculate the signal-to-noise ratio (SNR) of the selected ^{19}F signal intensity patch. Each ^{19}F MR image was processed in a way that only the pixels with an SNR of 3.5 or higher appear in the image (37), and the background noise was suppressed. SNR values of the ^{1}H images also were calculated for the same ROIs. ^{19}F SNR values were normalized to the corresponding ^{1}H ratios. A description of immunohistochemistry and histologic grading of inflammation and dysplasia can be found in Appendix E1 (online).

Statistical Analysis

Statistical analysis was performed by using a nonparametric Mann-Whitney test after a normal distribution test through histogram analysis and a Shapiro-Wilk test. For multigroup comparison (ascending colon vs descending colon, ^{19}F signal vs no signal), *P* values were adjusted with Bonferroni correction. A Spearman correlation factor was used as an indicator of correlation between ^{19}F signal intensity and total colitis score. A significance level of .05 (.05/3 for Bonferroni correction) was used for all statistical analysis. Statistical analysis was performed by using GraphPad Prism 5 software (GraphPad Software, La Jolla, Calif).

Results

In Vivo ^{19}F MR Imaging of Colon Inflammation

^{19}F MR imaging showed PFC emulsions accumulating in the colon wall, with a patchy distribution (Fig 1a). No ^{19}F signal could be detected in the colon wall of mice that did not have colitis-associated dysplasia (Fig 1b). To investigate the change of ^{19}F signal intensity over time, the SNR of ^{19}F signal in the colon wall was normalized to the SNR of corresponding ^{1}H images. Normalized SNR showed that ^{19}F signal intensity decreased over time but persisted for up to 110 days, at which time the animals were euthanized (Fig 1c). ^{19}F signals were also detected in the vertebra and spleen in all mice, reflecting normal macrophage activity.

Colocalization of ^{19}F Signal with Inflammatory and Dysplastic Lesions

The ^{19}F signals from ex vivo imaging were concentrated in the colon wall, showing several distinct foci (Fig 2a, 2b). The ^{19}F signal was more pronounced in the descending colon than in the ascending colon. Colon segments without ^{19}F signal (eight from the ascending colon, four from the descending colon) were also found (Fig 2c). Hemotoxylin-eosin–stained slices from paraffin-embedded tissues were then compared with the corresponding axial MR images. Strong ^{19}F signals could be observed in regions with severe inflammation, as characterized by abundant phagocytic immune cell infiltration or dysplastic lesions (Fig 2d).

Identification of Macrophages as the Source of ^{19}F MR Signal

Macrophages were found to infiltrate the lamina propria at the site of PFC accumulation (Fig E2a [online]). Images with higher magnification showed that PFC emulsions were almost exclusively present within the cytoplasm of macrophages, outside of the nucleus, and within the boundary of the cell membrane (Fig E2b–E2d [online]). However, not all macrophages

were labeled because of *(a)* the lack of PFC contact, *(b)* PFC excretion and dissipation, or *(c)* the presence of younger macrophages cells that infiltrated after the PFC was cleared from the circulation.

Correlation of ^{19}F Signal with Histologic Scores of Inflammation and Dysplasia

Sections of colon segments with ^{19}F signal exhibited more inflammation than did those without ^{19}F signal, as characterized by mononuclear cell infiltration and the appearance of a thick colon wall. For most of the parameters, the sections from colon segments with ^{19}F signal exhibited higher scores than did those without signal, especially for the mononuclear cell infiltration criteria (Fig E3 [online], Fig 3a). Dysplasia scores and total colitis scores also were compared. Segments with ^{19}F signal had significantly higher scores for both dysplasia (0.63 ± 0.81, P = .013) and colitis (3.06 ± 2.35, P = .006) (Fig 3b). Comparison of segments from the ascending colon and segments from the descending colon showed that the latter group had higher scores (Fig 4a).

For segments with ^{19}F signal, normalized ^{19}F SNR values were then correlated with corresponding histologic scores of colitis and dysplasia. ^{19}F signals from both the ascending colon and the descending colon showed a significant correlation with the total colitis score (Fig 4b, 4c; Table). The dysplasia groups had a significantly higher total colitis score and normalized ^{19}F SNR values (Fig 4d, 4e).

Discussion

In this study, we show as proof-of-principle that ^{19}F MR imaging can be used to track bowel inflammation and that its magnitude is associated with colitis-associated dysplasia development. In vivo MR imaging showed a patchy distribution of ^{19}F signal intensity in the colon wall, with colocalization of dysplastic lesions and ^{19}F-positive inflammatory sites. Histologic scores of inflammation and associated dysplasia showed a significant correlation with the intensity of the ^{19}F signal, indicating that the severity of inflammation can be noninvasively measured with MR imaging.

For measurement of ^{19}F signal intensity, the ^{19}F SNR was normalized to the SNR of the corresponding ^{1}H image. Hence, all factors involved in MR image acquisition that determine sensitivity, including coil sensitivity, field homogenization, and receiver gain, can be corrected for with this normalization, making it possible to compare ^{19}F signal intensities among different animals at various imaging time points. The normalized ^{19}F SNR from in vivo imaging showed a persisting ^{19}F signal intensity over time. Given the long life span of macrophages (38), this stable ^{19}F signal likely originated from macrophages that infiltrated during the start of inflammation. It is possible that PFC nanoparticles did exchange between macrophage populations; however, based on studies of iron oxide particles and macrophage transfer from labeled cells (39), the occurrence of transcellular transfer is expected to be minimal.

The correlation of normalized ^{19}F SNR to histologic disease scores suggests that ^{19}F signal represents the severity of inflammation and dysplasia development. The segment with ^{19}F signals had higher scores in most of the criteria used for inflammation assessment than did

segments without signals. The most prominent difference was observed in mononuclear cell infiltration criteria, while peripheral blood mononuclear cell infiltration criteria did not show a significant difference. This phenomenon further supports the selective in situ PFC labeling of macrophages, which was confirmed with immunohistochemistry. The total colitis score (ie, the sum of scores from all the criteria) was also well represented by normalized ^{19}F SNR values. The total colitis scores in the descending colon were significantly higher than those in the ascending colon. This finding is in agreement with findings of previous studies that showed that the descending colon is more damaged than the ascending colon when treated with dextran sulfate sodium and is more susceptible to tumor growth (36). All the adenomas and dysplastic lesions we observed were from the descending colon, further corroborating the well-established relationship between inflammation and cancer. When we compared descending colon segments with dysplasia and those without, we found that the former group had significantly higher total colitis scores and normalized ^{19}F SNR values.

Our study had several limitations. Most importantly, while we found a positive correlation between the severity of inflammation and the development of dysplasia, our approach is not a specific predictor for development of colitis-associated dysplasia, since dysplasia can be present in patients with IBD without active inflammation (40). While the duration and severity of inflammation is generally correlated with cancer development in patients with IBD (13), the inflammatory processes can be intermittent, with cancer development being stochastic. Our ^{19}F MR imaging approach cannot be used to distinguish inflammatory lesions from precancerous or cancerous lesions. Further studies are needed for instances in which ^{19}F MR imaging is combined with contrast material–enhanced and T2-weighted MR imaging to evaluate its relative sensitivity and specificity. While these studies are difficult to perform in mice, it should be noted that in patient studies, ^{19}F signal will not interfere with the conventional ^{1}H signal. While ^{19}F MR imaging cell tracking has recently entered the clinical realm, only the injection site could be visualized in patients when migrating dendritic cells were prelabeled ex vivo (34) and injected at a dose of 1×10^7 cells. The sensitivity of the detection of macrophages labeled in situ with a clinical set-up is not known. Our experiments were performed at 11.7 T, which is a high preclinical field strength, where the SNR is several-fold better as compared with the lower magnetic fields of conventional clinical imagers (1.5 or 3.0 T); thus, our results are not directly comparable with what would be expected at lower field strength. A potential drawback is the current limited availability of the needed hardware (dual ^{1}H- and ^{19}F-tuned coils and interfaces), making our approach not widely applicable. Also, the macrophage intracellular fluorine content is unknown. For labeled cells in general, this depends on cell size and the concentration and length of label incubation. For ex vivo prelabeled cells, this can be easily controlled and measured (with cells typically containing $[1–5] \times 10^{12}$ fluorine atoms per cell); however, one could further determine the fluorine content of in situ–labeled macrophages. One would have to harvest the tissue, make single cell suspensions, flow sort for macrophages (by virtue of the fluorescent perfluorocarbon), and perform a ^{19}F NMR experiment. The total dose of PFC that was administered to the mice in our study (1.6 g of PFC per kilogram of body weight) is within the range used in clinical studies in which a PFC emulsion (Oxygent; Alliance Pharmaceuticals, Chippenham, England) was used as an artificial red blood cell substitute to carry oxygen; when PFC is administered at a dose of

1.2–1.8 g/kg, an excellent safety profile was observed with unaltered immunologic parameters (41).

Practical applications

In summary, early diagnosis of colitis-associated dysplasia is an important factor for successful treatment of subsequent colitis–associated cancer, given its lower survival rate when compared with that of sporadic colorectal cancer (42). Since ^{19}F MR imaging is noninvasive and depends on macrophage infiltration rather than the macroscopic tissue appearance, it may be further applied as an adjunct technique to determine the risk of site-specific development of colitis-associated dysplasia.

Supplementary Material

Refer to Web version on PubMed Central for supplementary material.

Acknowledgments

The authors are grateful to the laboratory of Cory Brayton, DVM, for performing histologic scoring, and to Piotr Walczak, MD, and Irina Shats, MS, for their assistance with immunohistochemistry and microscopy.

Partially supported by the National Institutes of Health (U54 CA151838).

Abbreviations

IBD	inflammatory bowel disease
PFC	perfluorocarbon
RARE	rapid acquisition with relaxation enhancement
ROI	region of interest
SNR	signal-to-noise ratio

References

1. Coussens LM, Werb Z. Inflammation and cancer. Nature. 2002; 420(6917):860–867. [PubMed: 12490959]
2. Balkwill F, Charles KA, Mantovani A. Smoldering and polarized inflammation in the initiation and promotion of malignant disease. Cancer Cell. 2005; 7(3):211–217. [PubMed: 15766659]
3. Mantovani A, Allavena P, Sica A, Balkwill F. Cancer-related inflammation. Nature. 2008; 454(7203):436–444. [PubMed: 18650914]
4. Karin M. Nuclear factor-kappaB in cancer development and progression. Nature. 2006; 441(7092): 431–436. [PubMed: 16724054]
5. Yu H, Kortylewski M, Pardoll D. Crosstalk between cancer and immune cells: role of STAT3 in the tumour microenvironment. Nat Rev Immunol. 2007; 7(1):41–51. [PubMed: 17186030]
6. Balkwill F, Mantovani A. Inflammation and cancer: back to Virchow? Lancet. 2001; 357(9255): 539–545. [PubMed: 11229684]
7. Flossmann E, Rothwell PM, British Doctors Aspirin Trial and the UK-TIA Aspirin Trial. Effect of aspirin on long-term risk of colorectal cancer: consistent evidence from randomised and observational studies. Lancet. 2007; 369(9573):1603–1613. [PubMed: 17499602]

8. Tenesa A, Dunlop MG. New insights into the aetiology of colorectal cancer from genome-wide association studies. Nat Rev Genet. 2009; 10(6):353–358. [PubMed: 19434079]
9. Grivennikov SI. Inflammation and colorectal cancer: colitis-associated neoplasia. Semin Immunopathol. 2013; 35(2):229–244. [PubMed: 23161445]
10. Rubin DC, Shaker A, Levin MS. Chronic intestinal inflammation: inflammatory bowel disease and colitis-associated colon cancer. Front Immunol. 2012; 3:107. [PubMed: 22586430]
11. Terzić J, Grivennikov S, Karin E, Karin M. Inflammation and colon cancer. Gastroenterology. 2010; 138(6):2101–2114.e5. [PubMed: 20420949]
12. Ullman TA, Itzkowitz SH. Intestinal inflammation and cancer. Gastroenterology. 2011; 140(6): 1807–1816. [PubMed: 21530747]
13. Rutter M, Saunders B, Wilkinson K, et al. Severity of inflammation is a risk factor for colorectal neoplasia in ulcerative colitis. Gastroenterology. 2004; 126(2):451–459. [PubMed: 14762782]
14. Schreyer AG, Seitz J, Feuerbach S, Rogler G, Herfarth H. Modern imaging using computer tomography and magnetic resonance imaging for inflammatory bowel disease (IBD) AU1. Inflamm Bowel Dis. 2004; 10(1):45–54. [PubMed: 15058527]
15. Sempere GA, Martinez Sanjuan V, Medina Chulia E, et al. MRI evaluation of inflammatory activity in Crohn's disease. AJR Am J Roentgenol. 2005; 184(6):1829–1835. [PubMed: 15908538]
16. Weissleder R, Nahrendorf M, Pittet MJ. Imaging macrophages with nanoparticles. Nat Mater. 2014; 13(2):125–138. [PubMed: 24452356]
17. Modo M, Hoehn M, Bulte JW. Cellular MR imaging. Mol Imaging. 2005; 4(3):143–164. [PubMed: 16194447]
18. Kadayakkara DK, Ranganathan S, Young WB, Ahrens ET. Assaying macrophage activity in a murine model of inflammatory bowel disease using fluorine-19 MRI. Lab Invest. 2012; 92(4):636–645. [PubMed: 22330343]
19. Flögel U, Ding Z, Hardung H, et al. In vivo monitoring of inflammation after cardiac and cerebral ischemia by fluorine magnetic resonance imaging. Circulation. 2008; 118(2):140–148. [PubMed: 18574049]
20. van Heeswijk RB, Pellegrin M, Flögel U, et al. Fluorine MR imaging of inflammation in atherosclerotic plaque in vivo. Radiology. 2015; 275(2):421–429. [PubMed: 25496216]
21. Hitchens TK, Ye Q, Eytan DF, Janjic JM, Ahrens ET, Ho C. 19F MRI detection of acute allograft rejection with in vivo perfluorocarbon labeling of immune cells. Magn Reson Med. 2011; 65(4): 1144–1153. [PubMed: 21305593]
22. Temme S, Bönner F, Schrader J, Flögel U. 19F magnetic resonance imaging of endogenous macrophages in inflammation. Wiley Interdiscip Rev Nanomed Nanobiotechnol. 2012; 4(3):329–343. [PubMed: 22354793]
23. Jacoby C, Temme S, Mayenfels F, et al. Probing different perfluorocarbons for in vivo inflammation imaging by 19F MRI: image reconstruction, biological half-lives and sensitivity. NMR Biomed. 2014; 27(3):261–271. [PubMed: 24353148]
24. Ahrens ET, Bulte JWM. Tracking immune cells in vivo using magnetic resonance imaging. Nat Rev Immunol. 2013; 13(10):755–763. [PubMed: 24013185]
25. Ruiz-Cabello J, Barnett BP, Bottomley PA, Bulte JW. Fluorine (19F) MRS and MRI in biomedicine. NMR Biomed. 2011; 24(2):114–129. [PubMed: 20842758]
26. Bulte JW. Hot spot MRI emerges from the background. Nat Biotechnol. 2005; 23(8):945–946. [PubMed: 16082363]
27. Ruiz-Cabello J, Walczak P, Kedziorek DA, et al. In vivo "hot spot" MR imaging of neural stem cells using fluorinated nanoparticles. Magn Reson Med. 2008; 60(6):1506–1511. [PubMed: 19025893]
28. Barnett BP, Ruiz-Cabello J, Hota P, et al. Use of perfluorocarbon nanoparticles for non-invasive multimodal cell tracking of human pancreatic islets. Contrast Media Mol Imaging. 2011; 6(4): 251–259. [PubMed: 21861285]
29. Gaudet JM, Ribot EJ, Chen Y, Gilbert KM, Foster PJ. Tracking the fate of stem cell implants with fluorine-19 MRI. PLoS One. 2015; 10(3):e0118544. [PubMed: 25767871]

30. Mahida YR. The key role of macrophages in the immunopathogenesis of inflammatory bowel disease. Inflamm Bowel Dis. 2000; 6(1):21–33. [PubMed: 10701146]
31. Rugtveit J, Brandtzaeg P, Halstensen TS, Fausa O, Scott H. Increased macrophage subset in inflammatory bowel disease: apparent recruitment from peripheral blood monocytes. Gut. 1994; 35(5):669–674. [PubMed: 8200563]
32. Srinivas M, Turner MS, Janjic JM, Morel PA, Laidlaw DH, Ahrens ET. In vivo cytometry of antigen-specific t cells using 19F MRI. Magn Reson Med. 2009; 62(3):747–753. [PubMed: 19585593]
33. Ahrens ET, Young WB, Xu H, Pusateri LK. Rapid quantification of inflammation in tissue samples using perfluorocarbon emulsion and fluorine-19 nuclear magnetic resonance. Biotechniques. 2011; 50(4):229–234. [PubMed: 21548906]
34. Ahrens ET, Helfer BM, O'Hanlon CF, Schirda C. Clinical cell therapy imaging using a perfluorocarbon tracer and fluorine-19 MRI. Magn Reson Med. 2014; 72(6):1696–1701. [PubMed: 25241945]
35. Neufert C, Becker C, Neurath MF. An inducible mouse model of colon carcinogenesis for the analysis of sporadic and inflammation-driven tumor progression. Nat Protoc. 2007; 2(8):1998–2004. [PubMed: 17703211]
36. Thaker AI, Shaker A, Rao MS, Ciorba MA. Modeling colitis-associated cancer with azoxymethane (AOM) and dextran sulfate sodium (DSS). J Vis Exp. 2012 Sep 11.(67) pii: 4100.
37. Boehm-Sturm P, Mengler L, Wecker S, Hoehn M, Kallur T. In vivo tracking of human neural stem cells with ^{19}F magnetic resonance imaging. PLoS One. 2011; 6(12):e29040. [PubMed: 22216163]
38. Parihar A, Eubank TD, Doseff AI. Monocytes and macrophages regulate immunity through dynamic networks of survival and cell death. J Innate Immun. 2010; 2(3):204–215. [PubMed: 20375558]
39. Liu W, Frank JA. Detection and quantification of magnetically labeled cells by cellular MRI. Eur J Radiol. 2009; 70(2):258–264. [PubMed: 18995978]
40. Harpaz N, Polydorides AD. Colorectal dysplasia in chronic inflammatory bowel disease: pathology, clinical implications, and pathogenesis. Arch Pathol Lab Med. 2010; 134(6):876–895. [PubMed: 20524866]
41. Noveck RJ, Shannon EJ, Leese PT, et al. Randomized safety studies of intravenous perflubron emulsion. II. effects on immune function in healthy volunteers. Anesth Analg. 2000; 91(4):812–822. [PubMed: 11004031]
42. Watanabe T, Konishi T, Kishimoto J, et al. Ulcerative colitis-associated colorectal cancer shows a poorer survival than sporadic colorectal cancer: a nationwide Japanese study. Inflamm Bowel Dis. 2011; 17(3):802–808. [PubMed: 20848547]

Advances in Knowledge

- Intravenous injection of perfluorocarbons followed by in situ labeling of macrophages can be used to detect chronic bowel inflammation with fluorine 19 (^{19}F) MR imaging.
- A significantly ($P = .002$) higher normalized ^{19}F signal intensity is found at sites containing dysplastic tissue (mean, 0.58 ± 0.09) compared with sites without dysplasia development (mean, 0.17 ± 0.22).

Implication for Patient Care

- ^{19}F MR imaging can be used to assess the severity of bowel inflammation in patients with inflammatory bowel disease and may be further developed clinically as a noninvasive tool with which to determine the risk of developing colitis-associated dysplasia.

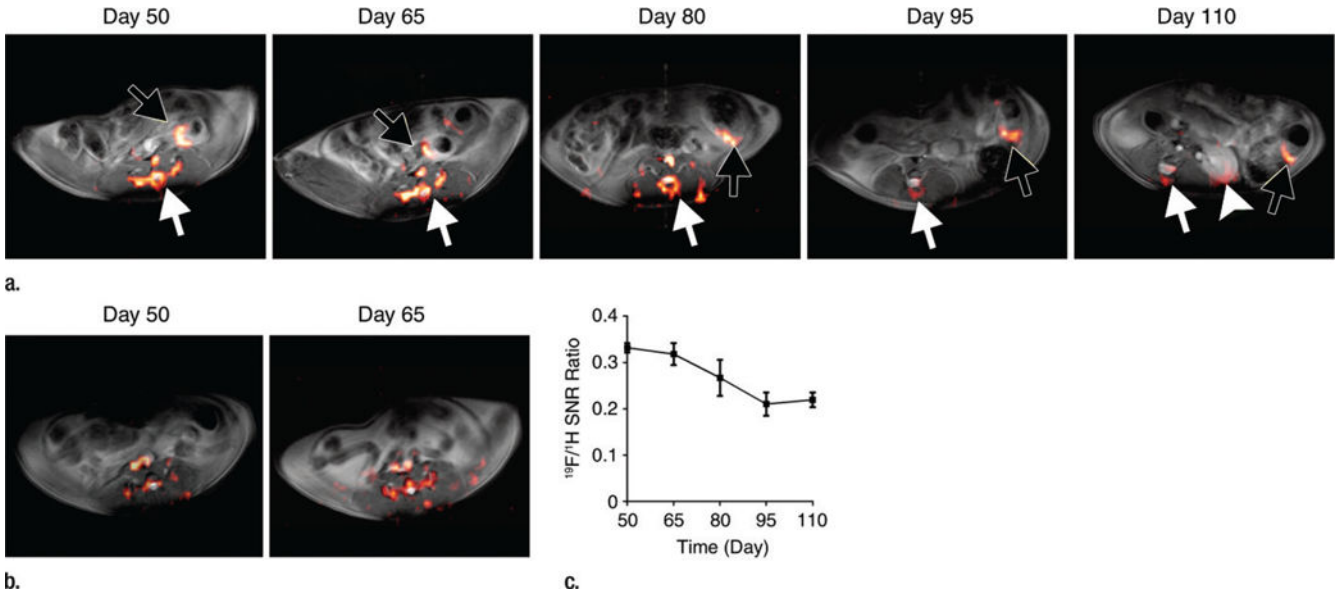

Figure 1.

(**a**) In vivo axial merged ^{1}H and ^{19}F MR images of the abdomen in mice with colitis-associated dysplasia obtained at different days. Accumulation of PFCs is visible in the colon (black arrows) and vertebrae (white arrows). ^{19}F signal intensity was also detected in the kidney at day 110 (arrowhead). (**b**) In vivo axial MR images in control mice at days 50 and 65 do not show ^{19}F signal intensity in the colon. The ^{19}F signal intensity is seen in only the vertebra and the iliac lymph nodes. PFC was injected on day 48, and no further PFC was given; therefore, control mice were not examined after day 65. (**c**) Graph shows normalized ^{19}F SNR in all ROIs combined. The ^{19}F signal intensity persisted over time. Error bars indicate standard error of the mean.

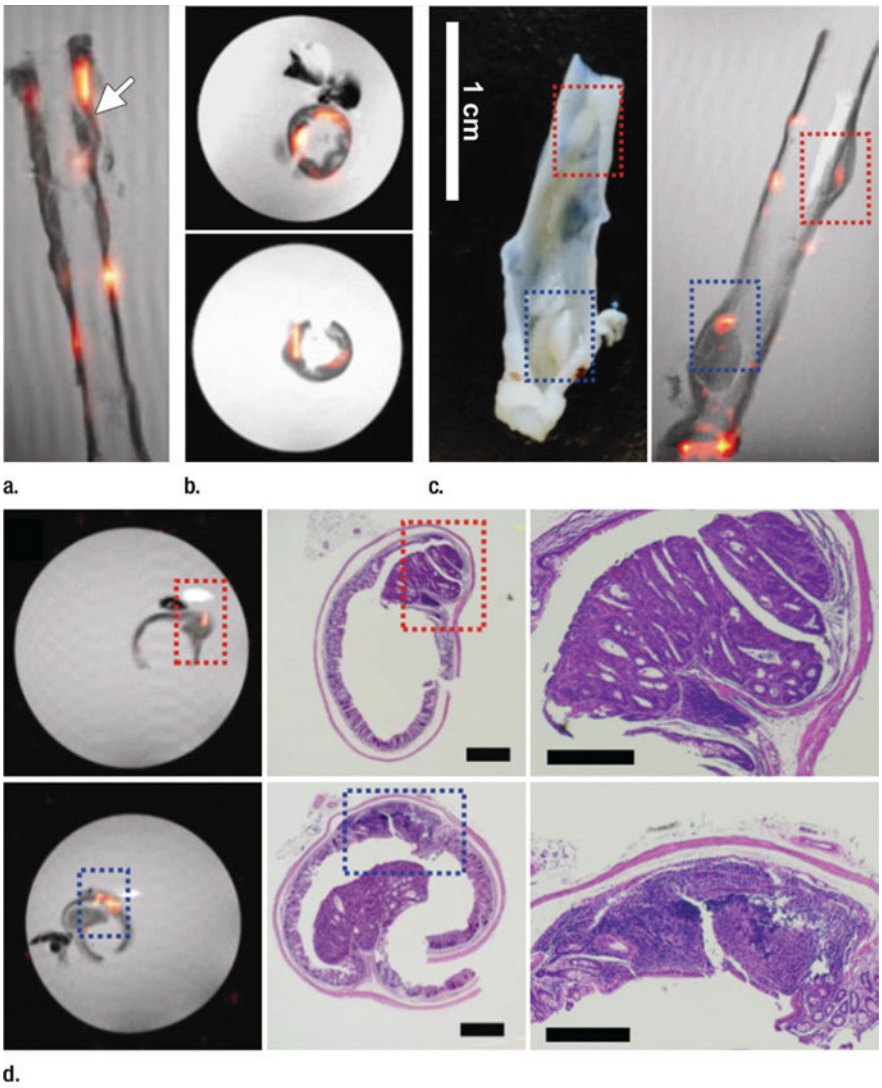

Figure 2.

Ex vivo MR imaging and colocalization of ^{19}F signals with adenoma and inflammatory sites. (**a**) Sagittal MR image of an excised descending colon. Note the adenoma growth (arrow) from a ^{19}F-positive inflammatory site. (**b**) Representative axial merged ^{1}H and ^{19}F MR images of the descending (top) and ascending (bottom) colon fixed in 4% paraformaldehyde. (**c**) Gross comparison of excised descending colon (left) and corresponding MR image (right). Red and blue boxes indicate two adenomas with corresponding gross and MR images (^{19}F signal intensity). (**d**) Axial ex vivo MR images of the descending colon (left) were compared with corresponding hematoxylin-eosin–stained slices (middle, right). Colocalization of ^{19}F signal intensity with either an adenoma (red box) or an inflammatory site (blue box) can be observed (scale bar = 500 μm and 300 μm for lower and higher magnifications, respectively).

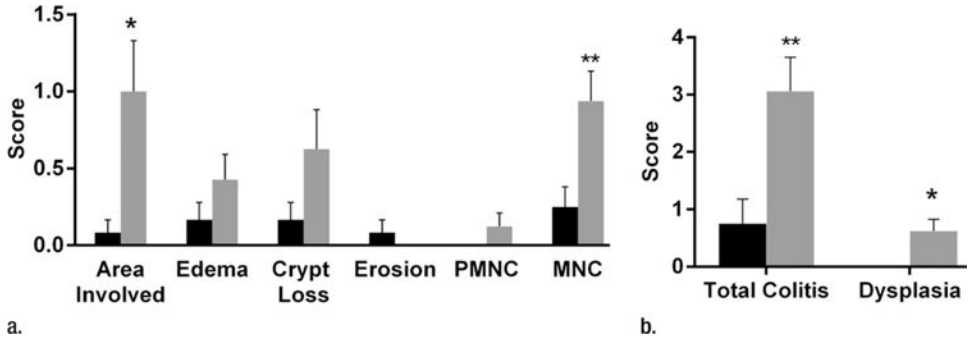

Figure 3.

(**a**) Graph shows colon segments with ^{19}F signal (gray) have higher histologic scores than do segments without ^{19}F signal (black) for most of the scoring parameters. Significant differences were observed for the area involved (* $P = .036$) and mononuclear cell *(MNC)* infiltration (** $P = .009$) criteria. *PMNC* = peripheral blood mononuclear cell. (**b**) Total colitis score was calculated by summation of the scores for all criteria. Graph shows colon segments with ^{19}F signal had significantly higher total colitis (* $P = .006$) and dysplasia (** $P = .013$) scores than did segments without ^{19}F signal. Error bars indicate standard error of the mean.

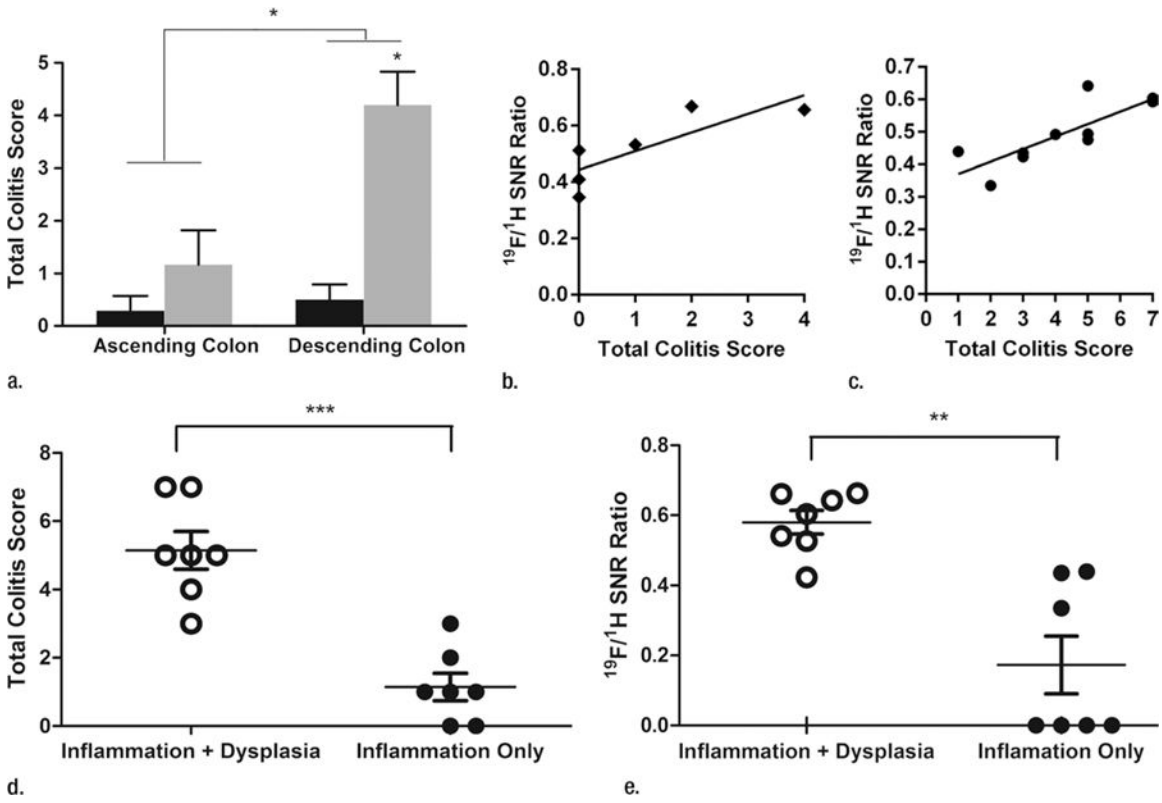

Figure 4.

Graphs show correlation between normalized ^{19}F SNR (calculated from ex vivo images) and histologic disease scores. Error bars indicate standard error of the mean. (**a**) Comparison of total colitis score between ascending colon ($n = 14$) and descending colon ($n = 14$). The descending colon exhibits significantly higher scores than does the ascending colon (* $P = .022$). Within the descending colon, segments with ^{19}F signal (gray, $n = 10$) have significantly higher scores than do those without signal (black, $n = 4$) (* $P = .016$). (**b**) Correlation between normalized ^{19}F SNR and total colitis score in ascending colon segments ($n = 6$ with ^{19}F signal) ($r = 0.88$, $P = .033$). (**c**) Graph shows correlation between normalized ^{19}F SNR with total colitis score in descending colon segments ($n = 10$ with ^{19}F signal) ($r = 0.82$, $P = .0058$). (**d**) Graph shows total colitis scores in descending colon segments with either inflammation and dysplasia ($n = 7$) or only inflammation ($n = 7$) (*** $P = .0025$). (**e**) Graph shows normalized ^{19}F SNR values in descending colon segments with either inflammation and dysplasia or only inflammation (** $P = .0023$).

Correlation of ^{19}F Signal to the Degree of Inflammation and Dysplasia

Histologic Score	Ascending Colon	Descending Colon
Total colitis	$r = 0.88$, $P = .033$	$r = 0.82$, $P = .0058$
Dysplasia	NA	$r = 0.67$, $P = .039$

Note.—NA = not applicable. (No ascending colon segments contained dysplasia.)